J. Quant. Spectrosc. Radiat. Transfer. Vol. 11, pp. 263–281. Pergamon Press 1971. Printed in Great Britain

UNIFIED THEORY CALCULATIONS OF STARK BROADENED HYDROGEN LINES INCLUDING LOWER STATE INTERACTIONS*

C. R. VIDAL, J. COOPER† and E. W. SMITH

National Bureau of Standards, Boulder, Colorado 80302

(*Received* 22 *July* 1970)

Abstract—Recently published calculations of hydrogen Stark broadening on the basis of the unified classical path theory have been extended to include lower state interactions in the final line profile. A detailed comparison with experiments in the density range 10^{13}–10^{17} cm^{-3} is given.

I. INTRODUCTION

IN A recent paper,[1] henceforth referred to as paper I, the unified classical path theory[2] was generalized for the case of upper and lower state interactions and was applied to the Stark broadening of hydrogen. The thermal average of the time development operator and the final intensity profile of any hydrogen line were derived for the general case including lower state interactions. Numerical calculations for the thermal average including lower state interactions have been presented. The calculations of the final line profiles, however, have so far been restricted to the Lyman lines. In this paper we discuss calculations of the intensity profile including lower state interactions which are more involved because they require the evaluation of tetradic operators and contain more extensive summations over vector coupling coefficients. The influence of lower state interactions is demonstrated for the first few lines of the Balmer series and possible simplifications for the higher series members are pointed out. A detailed comparison with various experiments covering the electron density range from about 10^{13}–10^{17} cm^{-3} is given requiring for low electron densities a convolution of the first series members with the Doppler profile. The unified theory calculations are also compared with static calculations. The applied computer program is presented in an NBS Monograph.[28]

II. BASIC RELATIONS

In this section we summarize briefly the basic relations, which have been derived in paper I and are used for the unified theory calculations presented in this paper.

* This research was supported in part by the Advanced Research Projects Agency of the Department of Defense, monitored by Army Research Office—Durham under Contract No. DA-31-124-AR0-D-139.

† Also at the Joint Institute for Laboratory Astrophysics and Dept. of Physics and Astrophysics, University of Colorado.

With the static ion field approximation the shape $I(\omega)$ of a Stark broadened line is given by

$$I(\omega) = \int_0^\infty P(\varepsilon_i) I(\omega, \varepsilon_i)\, \mathrm{d}\varepsilon_i, \tag{1}$$

where the normalized distribution function $P(\varepsilon_i)$ is the low frequency component of the fluctuating electric microfields. In this manner we regard the radiator as being an atom subjected to a static field ε_i and perturbed by the electrons. In the unified classical path theory[2] the ion field dependent line shape $I(\omega, \varepsilon_i)$ is obtained from

$$I(\omega, \varepsilon_i) = \frac{1}{\pi} \sum Im \left\{ \mathbf{d} \frac{1}{\Delta\omega_{\mathrm{op}}(\varepsilon_i) - \mathscr{L}[\Delta\omega_{\mathrm{op}}(\varepsilon_i)]} \mathbf{d} \right\}. \tag{2}$$

$\mathbf{d}$ is the dipole moment. The matrix elements of $\Delta\omega_{\mathrm{op}}$ specify the distance $\Delta\omega$ from a particular Stark component shifted by the static field ε_i and $\mathscr{L}$ is essentially the Fourier transform of the thermal average. Within the classical path approximation and the impact approximation $\mathscr{L}(\Delta\omega_{\mathrm{op}})$ is given by

$$\mathscr{L}(\Delta\omega_{\mathrm{op}}) = -i\Delta\omega_{\mathrm{op}} \int_0^\infty \exp(+it\Delta\omega_{\mathrm{op}}) \bar{\mathscr{F}}^{(1)}(t)\, \mathrm{d}t\, \Delta\omega_{\mathrm{op}} \tag{3}$$

where the thermal average

$$\bar{\mathscr{F}}^{(1)}(t) = n_e \int \mathrm{d}\mathbf{x}_1\, \mathrm{d}\mathbf{v}_1\, W(\mathbf{v}_1)[\mathscr{U}_1(\mathbf{R}, \mathbf{x}_1, \mathbf{v}_1, t) - 1]. \tag{4}$$

n_e denotes the electron density and W the velocity distribution function. The tetradic time development operator $\mathscr{U}_1$ is defined by the time ordered expression

$$\mathscr{U}_1(\mathbf{R}, \mathbf{x}_1, \mathbf{v}_1, t) = \mathscr{O} \exp\left\{ -\frac{i}{\hbar} \int_0^t \tilde{\mathscr{V}}_1(\mathbf{R}, \mathbf{x}_1, \mathbf{v}_1, t')\, \mathrm{d}t' \right\} \tag{5}$$

with the binary interaction

$$\tilde{\mathscr{V}}_1(\mathbf{R}, \mathbf{x}_1, \mathbf{v}_1, t) = \exp\{it\mathscr{H}_0/\hbar\} \mathscr{V}_1(\mathbf{R}, \mathbf{x}_1, \mathbf{v}_1, t) \exp\{-it\mathscr{H}_0/\hbar\}. \tag{6}$$

$\mathscr{V}_1$ is the Coulomb interaction potential between the radiator and a single perturbing electron. The Hamiltonian $\mathscr{H}_0$

$$\mathscr{H}_0 = \mathscr{H}_a + eZ\varepsilon_i \tag{7}$$

consists of the Hamiltonian $\mathscr{H}_a$ of the unperturbed radiator and the static ion part $eZ\varepsilon_i$. (For details see equations (IV. 16)–(IV. 18), (III. 14)–(III. 16) and (II. 2) of paper I.)

In evaluating the preceding equations for well isolated hydrogen lines we have to consider matrix elements only between states with the same principal quantum number n(no-quenching approximation) and it then is most convenient to work with parabolic states $|nqm\rangle$. m is the magnetic quantum number and the quantum number q is defined to be

$$q = n_1 - n_2 \tag{8}$$

with n_1 and n_2 being the usual parabolic quantum numbers which have to satisfy the relation

$$n = n_1 + n_2 + |m| + 1. \tag{9}$$

Furthermore, we distinguish quantum numbers which refer to the lower state from the upper state quantum numbers by a prime.

In taking matrix elements of the operators $\Delta\omega_{\rm op}$, $\mathbf{d}$ and $\mathscr{L}(\Delta\omega_{\rm op})$ between parabolic states it was shown in paper I that for the general case of upper and lower state interactions we have the following relations. For $\Delta\omega_{\rm op}$, which is diagonal in parabolic states, one obtains

$$\langle n'q'm'; nqm|\Delta\omega_{\rm op}|n'q'm'; nqm\rangle = \Delta\omega - \Delta\omega_i(n, q, n', q')\beta \tag{10}$$

where $\Delta\omega$ is the frequency perturbation from the position of the unperturbed line, β the normalized field strength in units of the Holtsmark field strength ε_0

$$\beta = \varepsilon_i/\varepsilon_0; \qquad \varepsilon_0 = \left(\frac{4\pi}{3}\right)^{2/3} e n_e^{2/3} \tag{11}$$

and

$$\Delta\omega_i(n, q, n', q') = \left(\frac{4\pi}{3}\right)^{2/3} \frac{3}{2}(nq - n'q')\frac{\hbar}{m} n_e^{2/3}. \tag{12}$$

$\Delta\omega_i$ is the frequency shift of a particular Stark component characterized by the quantum numbers n, q, n' and q' due to the Holtsmark field strength ε_0. The matrix elements of $\mathscr{L}(\Delta\omega_{\rm op})$ are given by

$$\langle n'q_b'm_b'; nq_bm_b|\mathscr{L}(\Delta\omega_{\rm op})|n'q_a'm_a'; nq_am_a\rangle = -i\pi[\Delta\omega - \Delta\omega_i(n, q_b, n', q_b')\beta]^2$$

$$\sum_{q_c q_c'} \langle n'q_b'm_b'; nq_bm_b|K(q_c, q_c')|n'q_a'm_a'; nq_am_a\rangle i(\Delta\omega, \beta, n, n', q_b, q_b', q_c, q_c') \tag{13}$$

where

$$\langle n'q_b'm_b'; nq_bm_b|K(q_c, q_c')|n'q_a'm_a'; nq_am_a\rangle = (-1)^{m_a + m_b} \sum_{l_a l_a' l_b l_b' L m_c m_c'} (2L+1)$$

$$\langle n'q_a'm_a'|n'l_a'm_a'\rangle\langle n'l_a'm_c'|n'q_c'm_c'\rangle\langle n'q_c'm_c'|n'l_b'm_c'\rangle\langle n'l_b'm_b'|n'q_b'm_b'\rangle$$

$$\langle nq_am_a|nl_am_a\rangle\langle nl_am_c|nq_cm_c\rangle\langle nq_cm_c|nl_bm_c\rangle\langle nl_bm_b|nq_bm_b\rangle$$

$$\begin{pmatrix} l_a' & l_a & L \\ -m_c' & m_c & M' \end{pmatrix}\begin{pmatrix} l_a' & l_a & L \\ -m_a' & m_a & M \end{pmatrix}\begin{pmatrix} l_b' & l_b & L \\ -m_c' & m_c & M' \end{pmatrix}\begin{pmatrix} l_b' & l_b & L \\ -m_b' & m_b & M \end{pmatrix}. \tag{14}$$

The unitary transformation $\langle nlm|nqm\rangle$ from parabolic to spherical states can be expressed in terms of $3j$-symbols[3]

$$\langle nlm|nqm\rangle = (-1)^{\frac{1}{2}(1+m-q-n)}\sqrt{(2l+1)}\begin{pmatrix} \frac{n-1}{2} & \frac{n-1}{2} & l \\ \frac{m-q}{2} & \frac{m+q}{2} & -m \end{pmatrix}. \tag{15}$$

Introducing the normalized time

$$s = \tilde{\omega}_p t \tag{16}$$

and the normalized frequency

$$\Delta\omega_R = [\Delta\omega - \Delta\omega_i(n, q_b, n', q_b')\beta]/\tilde{\omega}_p \tag{17}$$

with $\tilde{\omega}_p = \sqrt{(8\pi n_e e^2/m)}$ being the plasma frequency, the Fourier transform of the thermal average is defined to be

$$i(\Delta\omega_R, \beta, n, n', q_b, q_b', q_c, q_c') = \lim_{\varepsilon \to 0} \frac{1}{\pi} \int_0^\infty \exp[(-\varepsilon + i\Delta\omega_R)s]\bar{F}(s, n, q_c, n', q_c')\, ds. \tag{18}$$

The thermal average $\bar{F}(s)$ was evaluated in paper I for the general case of upper and lower state interactions and it was shown that $\bar{F}(s)$ may be approximated by a function $G(s) = \Sigma_k G_k(s)$ whose Fourier transform can be given analytically such that

$$i(\Delta\omega_R) = \sum_k i(k, \Delta\omega_R). \tag{19}$$

For most practical situations it turns out to be sufficient to consider only the first term in the series

$$i(k = 1, \Delta\omega_R) = a_1 b_1^2 e^{-iZ_1}\left\{iH_0^{(1)}(Z_1) + H_1^{(1)}(Z_1)\left[1 - \frac{i}{2Z_1}\right]\right\} \tag{20}$$

where $H_0^{(1)}$ and $H_1^{(1)}$ are Hankel functions and

$$Z_1 = b_1 \Delta\omega_R, \tag{21}$$

because the higher order terms usually affect the final line profile by not more than 2 per cent around $\Delta\omega \simeq \tilde{\omega}_p$. The constants a_1 and b_1 are given by

$$a_1 = -4\sqrt{(\pi)} n_e D^3 C^2 [B - \ln(4C^2)] \tag{22}$$

$$b_1 = \frac{9}{4\pi^2} C[B - \ln(4C^2)]^2, \tag{23}$$

where D is the Debye length, B a constant of the order of unity (see Table II in the appendix of paper I) and

$$C = \frac{3}{2}(nq - n'q')\frac{\hbar}{mDv_{av}}. \tag{24}$$

Finally we give for completeness the matrix elements of $\mathbf{d} \otimes \mathbf{d}$

$$\begin{aligned}
&\langle n'q_a'm_a'; n'q_b'm_b'|\mathbf{d} \otimes \mathbf{d}|nq_am_a; nq_bm_b\rangle \\
&\quad = (-1)^{m_a'} \sum_{l_a l_a'} \langle n'q_a'm_a'|n'l_a'm_a'\rangle\langle nl_am_a|nq_am_a\rangle \begin{pmatrix} l_a' & l_a & 1 \\ m_a' & -m_a & \mu \end{pmatrix}\begin{pmatrix} l_a' & l_a & 1 \\ 0 & 0 & 0 \end{pmatrix} \\
&[(2l_a+1)(2l_a'+1)]^{1/2}\langle nl_a|r|n'l_a'\rangle \\
&\quad (-1)^{m_b'} \sum_{l_b l_b'} \langle n'q_b'm_b'|n'l_b'm_b'\rangle\langle nl_bm_b|nq_bm_b\rangle \begin{pmatrix} l_b' & l_b & 1 \\ m_b' & -m_b & \mu \end{pmatrix}\begin{pmatrix} l_b' & l_b & 1 \\ 0 & 0 & 0 \end{pmatrix} \\
&\quad [(2l_b+1)(2l_b'+1)]^{1/2}\langle nl_b|r|n'l_b'\rangle
\end{aligned} \tag{25}$$

where the radial matrix elements are given in equation (63.2) of BETHE and SALPETER.[4]

In case of no lower state interaction where the time development operator between lower states is replaced by a unit operator the matrix elements of $\mathscr{L}(\Delta\omega_{op})$ in equations (13) and (14) simplify significantly and we have

$$\langle n'q'm'; nq_bm|\mathscr{L}_u(\Delta\omega_{op})|n'q'm'; nq_am\rangle = -i\pi[\Delta\omega-\Delta\omega_i(n, q_b, n', q')\beta]^2 \sum_{q_c}\langle nq_bm|K_u(q_c)|nq_am\rangle i(\Delta\omega, \beta, n, n', q_b, q', q_c) \tag{26}$$

where

$$\langle nq_bm|K_u(q_c)|nq_am\rangle = \sum_{l_a, m_c}\frac{1}{2l_a+1}\langle nq_am|nl_am\rangle\langle nq_bm|nl_am\rangle[\langle nl_am_c|nq_cm_c\rangle]^2. \tag{27}$$

Equation (26) simplifies even further for the Lyman lines with $|n'q'm'\rangle = |100\rangle$. For this case numerical calculations were given in paper I.

III. PROPERTIES OF THE $\mathscr{L}$ AND K MATRIX

In equations (13) and (26) we have split the $\mathscr{L}$-matrix into two parts. One part, the K-matrix, contains all the vector coupling coefficients or $3j$-symbols and is independent of the plasma parameters, while the other part, the Fourier transform of the thermal average $i(\Delta\omega)$, contains all the broadening parameters. The K-matrix is completely specified by the upper and lower state principal quantum numbers n and n' and needs to be calculated only once for every hydrogen line.

From equation (14) we realize first of all that the K-matrix is symmetric to the diagonal

$$\langle n'q_b'm_b'; nq_bm_b|K(q_c, q_c')|n'q_a'm_a'; nq_am_a\rangle = \langle n'q_a'm_a'; nq_am_a|K(q_c, q_c')|n'q_b'm_b'; nq_bm_b\rangle \tag{28}$$

while the $\mathscr{L}$-matrix is not, due to the factor $[\Delta\omega-\Delta\omega_i(n, q_b, n', q_b')\beta]^2$. Next we see from the $3j$-symbols that K is diagonal in the quantum number M.

$$M = m_a'-m_a = m_b'-m_b \tag{29}$$

Hence we may arrange the K-matrix and also the $\mathscr{L}$-matrix in such a manner that they are block diagonal in M, where $M = 0, \pm1, \pm2, \ldots, n+n'-2$. We also notice that matrix elements which differ only in the sign of M are identical.

$$\langle n'q_b'-m_b'; nq_b-m_b|K(q_c, q_c')|n'q_a'-m_a'; nq_a-m_a\rangle = \langle n'q_b'm_b'; nq_bm_b|K(q_c, q_c')|n'q_a'm_a'; nq_am_a\rangle. \tag{30}$$

Consequently, blocks which differ in the sign of M, can also be made identical. This greatly simplifies the matrix inversion required by equation (2). The problem is further simplified by the fact that also the $\mathbf{d}\otimes\mathbf{d}$-matrix can be made block diagonal in

$$\mu = m_a-m_a' = m_b-m_b', \tag{31}$$

where μ can only take on the values 0 and ± 1. As a result we finally have to evaluate only the blocks with $M = 0$ and $M = 1$ of the K and $\mathscr{L}$-matrix, respectively, because the block with $M = -1$ gives identically the same contribution to the final line profile as the block with $M = 1$ and all the other blocks with $|M| > 1$ do not contribute due to the $\mathbf{d} \otimes \mathbf{d}$ matrix. Further useful symmetry properties of the K-matrix are given in the following equations

$$\begin{aligned}\langle n' q_b' m_b'; n q_b m_b | K(q_c, q_c') | n' q_a' m_a'; n q_a m_a \rangle \\ = \langle n' - q_b' - m_b'; n - q_b - m_b | K(q_c, q_c') | n' - q_a' - m_a'; n - q_a - m_a \rangle \\ = \langle n' q_b' m_b'; n q_b m_b | K(-q_c, -q_c') | n' q_a' m_a'; n q_a m_a \rangle .\end{aligned} \tag{32}$$

The latter relation simplifies our summation over q_c and q_c' in equation (13) because also for the Fourier transform $i(\Delta\omega)$ we have

$$i(\Delta\omega, \beta, n, n', q_b, q_b', q_c, q_c') = i(\Delta\omega, \beta, n, n', q_b, q_b', -q_c, -q_c'). \tag{33}$$

In calculating $I(\omega, \varepsilon_i)$ according to equation (2) we always have to invert complex matrices. Since for computational purposes it is more convenient to work with real matrices and since we need only the imaginary part of the inverted matrix we make use of the following relations

$$X + iY = [A + iB]^{-1}$$

where

$$\begin{aligned} X &= [A + BA^{-1}B]^{-1} \\ Y &= -[B + AB^{-1}A]^{-1} \end{aligned} \tag{34}$$

with X, Y, A and B being real matrices. From equations (2), (13) and (18) it is clear that A contains the diagonal matrix of $\Delta\omega_{\text{op}}$ and the sine transform of the thermal average and B the cosine transform of the thermal average. In the limit of large $\Delta\omega$ we have

$$A = B + \Delta\omega \,.\, \mathrm{I} \tag{35}$$

(see equation (X. 18) of paper I) which simplifies to lowest order the Y-matrix to

$$Y \simeq -B/\Delta\omega^2. \tag{36}$$

This is the one electron limit, which as pointed out already in Section IV of paper I, does not require a matrix inversion.

IV. THE INFLUENCE OF LOWER STATE INTERACTIONS AND THE STATIC LIMIT

In the Figs. 1, 2, 3, 7 and 8 the intensity of the line is plotted vs. the frequency perturbation $\Delta\omega$ in units of the plasma frequency $\tilde{\omega}_p = \sqrt{(8\pi n e^2/m)}$. The frequency scale is preferred, because it represents essentially the energy perturbation and is therefore more meaningful for the discussion of Stark broadening than, for example, the wavelength scale, which is usually more convenient in the measurement. Furthermore, $\Delta\omega/\tilde{\omega}_p \lesssim 1$ is essentially the domain of the unmodified impact theory.

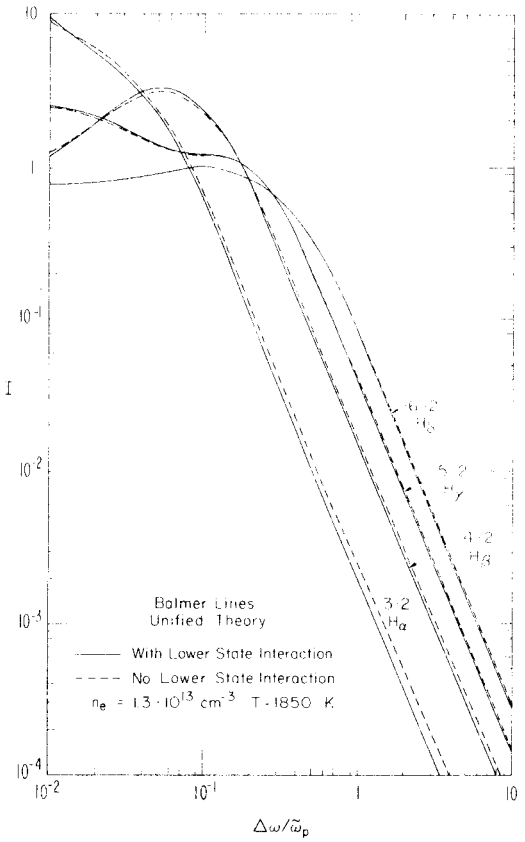

FIG. 1. The influence of lower state interactions on the Balmer lines H_α to H_δ.

We first demonstrate the influence of lower state interaction on the final line profile in Figs. 1 and 2 and compare three different methods of evaluation. In the first, most general method lower state interactions are taken into account and the line profiles are calculated on the basis of equations (13) and (14) using the correct Stark effect for electrons and ions (solid curves in Fig. 1). In the second method based on equations (26) and (27) we neglect lower state interactions for the electrons, i.e. we do not allow for perturbations of the lower state sublevels by electrons (dashed curves in Fig 1, solid curves in Fig. 2). However, we still use the correct Stark effect for the static ions. In the third and simplest method the line profiles are calculated like in case of the Lyman lines with no influence of the lower state for the electrons as well as the static ions (dashed curves in Fig. 2). These Lyman profiles were presented already in Paper I.

We realize first of all from Fig. 1 that in view of the accuracy to be expected from the unified classical path theory we may neglect lower state interaction due to the electrons for H_δ and therefore also for all the higher Balmer lines. For $n_e = 1.3 \cdot 10^{13}\,\mathrm{cm}^{-3}$ and $T = 1850°\mathrm{K}$ the biggest calculated difference between the cases with and without lower state interaction is 43 per cent for H_α, 10 per cent for H_β, 6 per cent for H_γ and 4 per cent

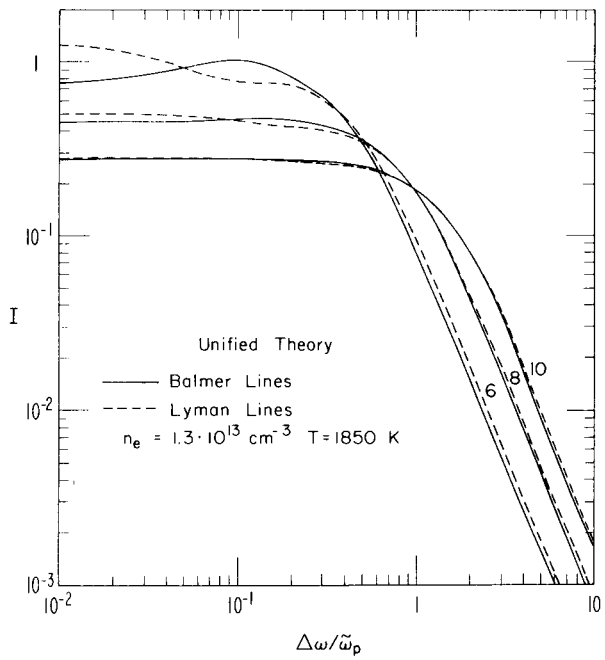

FIG. 2. Comparison of the Balmer and Lyman lines with the upper state principal quantum numbers $n = 6$, 8 and 10.

for H_δ. These differences have been obtained for the distant, almost quasistatic wing. They become slightly smaller in the purely static wing and are significantly smaller in the line center (14 per cent for H_α, 9 per cent for H_β, 3 per cent for H_γ and 2 per cent for H_δ). Similar differences may be obtained at any electron density and temperature. In the distant, purely static wing the difference will always be identical (39.2 per cent for H_α, 9.3 per cent for H_β, 5.7 per cent for H_γ and 3.6 per cent for H_δ), because the static ions are treated in both cases with the same, correct Stark effect, while the static electrons are treated in the second method with the Stark effect of the corresponding Lyman line.

In Fig. 2 the Balmer lines and the Lyman lines with the upper state principal quantum numbers $n = 6$, 8 and 10 are compared. In the line center we recognize the fact that the even Balmer lines have no unshifted Stark component, while the even Lyman lines do. The difference in the wings is also clear from the Stark effect of the Balmer and Lyman lines (see also Table 1 of the paper by VIDAL[5]). It therefore becomes apparent that for principal quantum numbers of about $n > 10$ one may neglect the influence of the lower states on the final line profile altogether and use the Lyman profiles throughout.

Next we compare in Fig. 3 the results of the unified classical path theory (solid curves) with quasistatic calculations (dashed curves) in order to show to what extent quasistatic calculations may be useful. The even Balmer lines up to $n = 14$ are plotted. The quasistatic profiles are based on the low frequency component of the electric microfield distribution functions[6,7] with a shielding parameter

$$r_0/D = 0.0898 n_e^{1/6}/\sqrt{T} \tag{37}$$

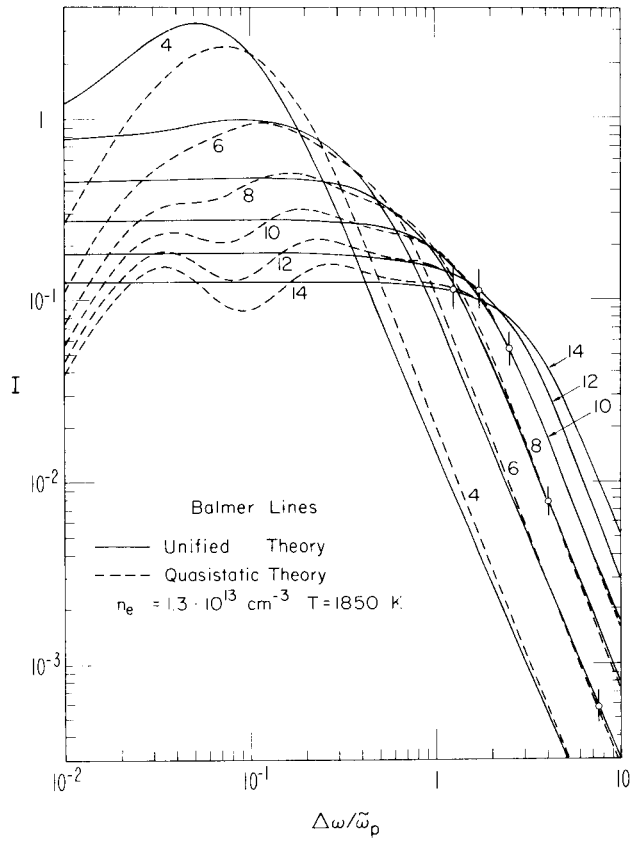

FIG. 3. Comparison of the unified theory and the quasistatic theory for the even Balmer lines with $n = 4$ to $n = 14$.

and the total density N being $N = 2n_e$. In addition, short vertical lines mark the position of the average Weisskopf frequency

$$\Delta\omega_c = 2mv_{av}^2/(3\pi^2\bar{n}_k\hbar) \tag{38}$$

as defined by UNSÖLD,[8] where the average splitting

$$\bar{n}_k = \sum_k n_k f_k / \sum_k f_k \tag{39}$$

with f_k being the oscillator strength of the k-th Stark component is frequently approximated by $\bar{n}_k \simeq n(n-1)/2$ (see also Table 1 of the paper by EDMONDS *et al.*[9]). The Weisskopf frequency indicates the domain of the quasistatic theory and there have been various estimates, which all agree within a factor of 2 to 3. From Fig. 3 it is apparent that with increasing principal quantum numbers the profiles based on the unified classical path theory approach more and more the static profiles and that the Weisskopf frequency turns out to be a rather conservative estimate for the useful range of the quasistatic theory. In the example presented we recognize that except for the very line center one may use

quasistatic calculations almost throughout the entire profile for principal quantum numbers of $n \gtrsim 10$. For practical purposes the hole in the center of the static profile and the structure in the line center, which for the higher series members appears to oscillate around the profile based on the unified classical path theory, will be smeared out by a convolution with the Doppler profile.

V. COMPARISON WITH EXPERIMENTS AND OTHER THEORIES

We start our comparison of the unified theory with experiments in the high and low electron density range with recent measurements by WIESE *et al.*[10] performed on a high current, wall-stabilized arc. The experimental set up and the method of evaluation is similar to the one described by WIESE *et al.*[11] However, a number of refinements are incorporated in the experimental set up and the achievable accuracy has been greatly improved.

In Figs. 4 and 5 the red and blue wings of the measured H_β and H_γ-profiles are plotted (solid lines), which have been obtained in the same run assuring the same electron density and temperature for both profiles. For the moment we do not consider the asymmetries of the profile, since the theory is not yet arranged to describe them. The electron density and temperature for this particular run have been determined in several ways from the absolute intensity of H_β with

$$n_e = 7.5 \cdot 10^{16}\,\mathrm{cm}^{-3} \qquad T = 12\,570°\mathrm{K},$$

from the absolute intensity of H_γ with

$$n_e = 7.7 \cdot 10^{16}\,\mathrm{cm}^{-3} \qquad T = 12\,640°\mathrm{K}$$

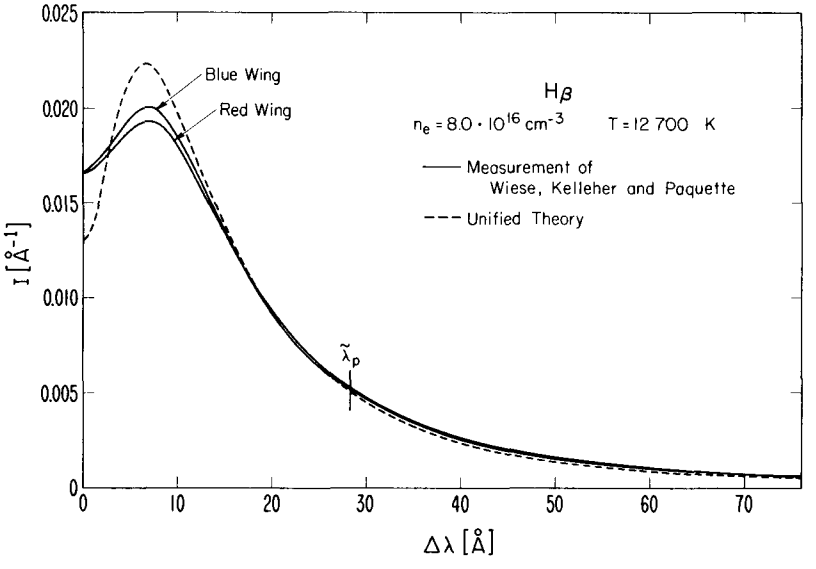

FIG. 4. Comparison between the unified theory for H_β and the experimental profile as measured by Wiese, Kelleher and Paquette.

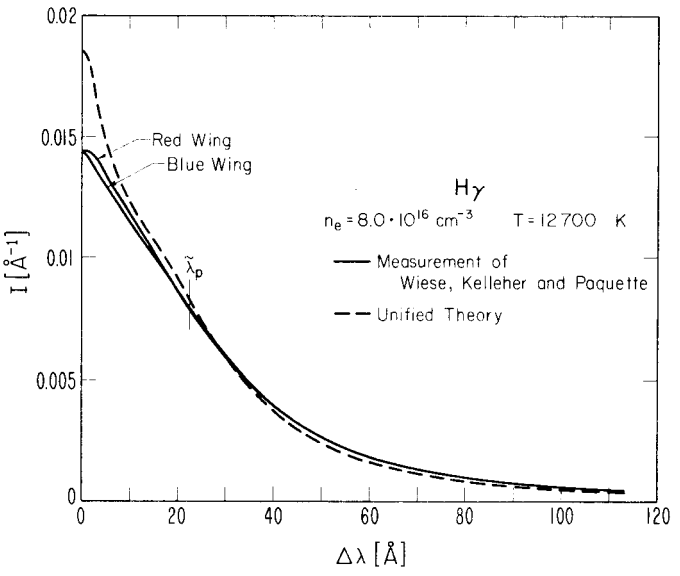

FIG. 5. Comparison between the unified theory for H_γ and the experimental profile as measured by Wiese, Kelleher and Paquette.

and from the absolute intensity of the continuum in the visible and in the UV, which differ by the contribution from the Balmer continuum, with

$$n_e = 8.0 \cdot 10^{16}\,\mathrm{cm}^{-3} \qquad T = 12\,730°\mathrm{K}.$$

The three values of the electron density differ in all runs by similar amounts. In particular the difference between the values from the H_β- and the continuum intensity is very reproducable and gives rise to a 6 per cent difference in the electron density. These are indications (private communication of Dr. Wiese) that these differences may be due to small Non LTE effects in the arc because of its rather small dimension. This would be consistent with the validity criteria for LTE in inhomogeneous stationary plasmas (see section 6–10 of GRIEM[12]). Since the continuum intensity is least affected the electron density and temperature as obtained from the continuum have been adopted as the best values in particular since the same values have been obtained from the continuum in the visible and the UV. For these parameter values the profiles as calculated with the unified theory including lower state interactions have been plotted in Figs. 4 and 5 with the same normalization $\int_{-\infty}^{+\infty} I(\Delta\lambda)\,\mathrm{d}\lambda = 1$ as the experimental profiles. We realize that the calculated profiles are slightly higher and narrower than the measured profiles. In *both* cases, however, the best agreement between theory and experiment in a least squares sense has been obtained with $8.5 \cdot 10^{16}\,\mathrm{cm}^{-3}$ meaning that the theoretical value appears to be 6 per cent larger than the experimental value.

Applying recent calculations of KEPPLE and GRIEM[13] one obtains from the half-, quarter- and eighth-width $n_e = 7.38 \cdot 10^{16}\,\mathrm{cm}^{-3}$ for H_β and $n_e = 8.05 \cdot 10^{16}\,\mathrm{cm}^{-3}$ for H_γ (as evaluated by Dr. Wiese), which reveals an intrinsic inconsistency because the two electron densities differ by about 10 per cent.

We also notice that the worst agreement is in the very line center, a feature which is so far common to all impact theories. This fact makes the determination of the electron density on the basis of fractional widths rather questionable because its definition may be ambiguous and it effectively normalizes wing intensities with respect to the intensity in the very line center, where the theory seems to be least reliable. Although this is the most convenient and most widely used method, it is definitely preferable to determine the electron density from a least squares fit of the experimental and theoretical profile using the same normalization for both profiles.

In Fig. 6 the calculations of KEPPLE and GRIEM[13] are compared with our calculations for H_β and $n_e = 6.4 \cdot 10^{16}\ \mathrm{cm}^{-3}$ and $T = 12\,200°\mathrm{K}$ indicating that our profile is narrower and higher hence giving rise to larger electron densities. In the very line center the most important difference appears to be due to the constant B in equations (22) and (23). While our calculations are based on a quantum number dependent constant B for a lower cutoff $\rho_{\min} = \hat{\lambda} + \frac{3}{2}n^2 a_0$, which has been selected according to the validity criterion of the classical path theory, Kepple and Griem use a larger value $B = 1.27$ for all the Stark components. We have repeated our calculations with their value of the constant B. The profile is included in Fig. 6 and does not quite agree with their calculations. It should be pointed out that the normalization of the profile of Kepple and Griem is slightly too small, which may account for part of the remaining difference in the very line center, where the unified classical path calculations should go over to the results of the impact theory, if the ion field dependent cut off (see equation VI.4 of paper I) is neglected.

From the preceding comparison we realize that at this stage the most important problem seems to be to obtain better values of the constant B whose dependence on various cutoff procedures was discussed in the Appendix of paper I for classical path theories

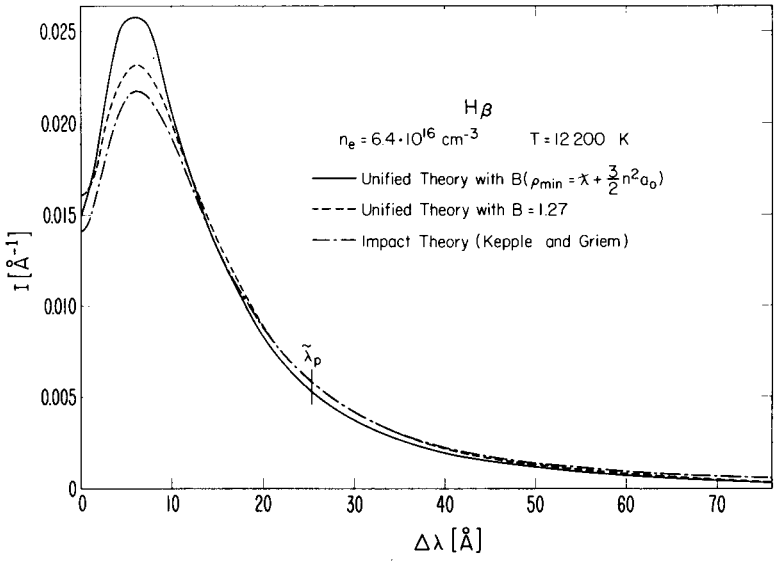

FIG. 6. Comparison between the unified theory with B as obtained for $\rho_{\min} = \hat{\lambda} + \frac{3}{2}n^2 a_0$, with $B = 1.27$ as used by Kepple and Griem and the modified impact theory of Kepple and Griem.

neglecting time ordering. We note that in case of the H_β and H_γ profiles in Figs. 4 and 5, better agreement between theory and experiment may be obtained with a constant B larger than that used in this paper, and that in case of the Lyman-α experiment of BOLDT and COOPER[14] discussed in paper I, better agreement is obtained with a smaller constant B.

For the moment we postpone the discussion of the various possibilities, which may affect the constant B, until we also have compared our results with measurements of the Balmer lines H_3–H_{14} and the Paschen lines P_6–P_{13} performed by VIDAL.[5,15] Unfortunately, these experiments do not provide an independent electron density measurement, which is as accurate as the measured profiles. Since, however, the measurements revealed a $\Delta\omega^{-5/2}$-wing, which for most of the lines extended over two orders of magnitude in intensity, the electron density was determined assuming that these measured $\Delta\omega^{-5/2}$-wings were identical to the asymptotic Holtsmark wings. In this manner the same electron density of $n_e = 1.3 \cdot 10^{13}\,\mathrm{cm}^{-3}$ was obtained within ± 4 per cent for all the Balmer lines from H_4 to H_{14} (see VIDAL[5]). In paper I it was pointed out (on the basis of the Lyman line calculations) that the unified theory calculations actually give the $\Delta\omega^{-5/2}$-wings which were measured in the experiment and which extend much further into the line center than a quasistatic theory would predict. However, over the intensity range measured, these $\Delta\omega^{-5/2}$-wings do not necessarily coincide with the asymptotic Holtsmark wing.

In the following we reevaluate the measured line profiles employing now the complete line profile from the line center to the wings. We concentrate primarily on the Balmer lines, which have been measured more accurately than the Paschen lines and where we also have more series members available. The measurements were performed on a stationary radio frequency discharge within a magnetic bottle as described by SCHLÜTER.[16] The electron temperature, which within the error limits is equal to the ion temperature, was measured to be $T = 1850°\mathrm{K}$. Consequently, we have to consider first of all to what extent Doppler broadening and the Zeeman effect may influence the first series members. In Fig. 7 the theoretical line profiles are shown for $n_e = 1.3 \cdot 10^{13}\,\mathrm{cm}^{-3}$ and $T = 1850°\mathrm{K}$ before (dashed lines) and after (solid lines) the convolution with the Doppler profile. It shows that up to around H_8 Doppler broadening has to be taken into account. In estimating the influence of the Zeeman effect we notice that for a magnetic field of 1800 Gauss (0.18 Tessla) as typically used in the experiments the separation of the outer components of the Lorentz triplet amounts to $0.168\,\mathrm{cm}^{-1}$. Neglecting complications due to the combined Zeeman and Stark effect this indicates that from around H_7 (full half width $= 1.76\,\mathrm{cm}^{-1}$) we may neglect the Zeeman effect for all the higher series members.

A comparison of the experimental and theoretical profiles for the Balmer lines H_7–H_{14} gives the best agreement for $n_e = 1.15 \cdot 10^{13}\,\mathrm{cm}^{-3}$, a value which is slightly smaller than the value of $n_e = 1.3 \cdot 10^{13}\,\mathrm{cm}^{-3}$ given by VIDAL.[5] This is not surprising because within the measured intensity range the apparent $\Delta\omega^{-5/2}$-wings of the unified theory calculations are all lying above the asymptotic Holtsmark wings on which the electron density value of VIDAL[5] was based. For this new value the measured and calculated Balmer lines H_7–H_{14} all agree within 5 per cent over the entire line profile. These maximum deviations are comparable to the achieved accuracies of the measurement and are so small that they hardly show up in a plot like in the Figs. 1, 2, 3, 7 and 8. For the lower Balmer lines only the line wings can be evaluated since the line center is noticeably affected by the Zeeman effect not included in the calculations. The agreement is not quite as good. However, the differences do not exceed 10 per cent for the wings of H_β to H_δ, which appears to be partially

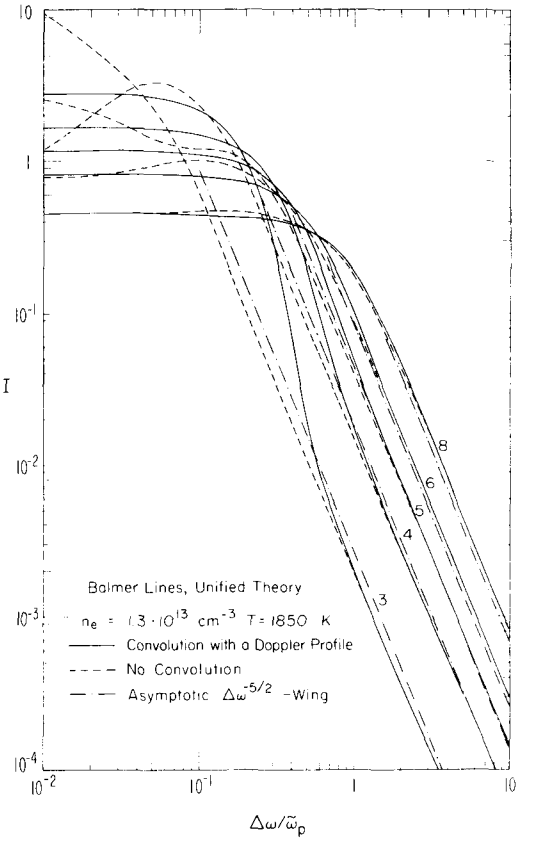

FIG. 7. The Balmer line profiles as calculated with the unified theory for $n_e = 1.3 \cdot 10^{13}$ cm^{-3} and $T = 1850$ °K with and without the convolution of the Doppler profile.

due to the growing influence of the apparatus profile for the narrower profiles of the lower series members.

In Fig. 8 our calculations are compared with the calculations of KEPPLE and GRIEM,[13] which have been extended to H_{12} by BENGTSON *et al.*[17] We see that their profiles are wider and that the higher series members do not show the measured $\Delta\omega^{-5/2}$-wings. From a comparison with Fig. 3 we also realize that with increasing principal quantum number n our profiles approach the static profiles while the profiles of Kepple and Griem do not. Their profiles actually appear to differ more and more from the static profiles with increasing principal quantum number n, which manifests the fact that the modified impact theory is not able to describe the static electrons.

As pointed out already in paper I, we emphasize again that contrary to the H_β- and H_γ-profiles discussed above, the higher series members are insensitive to the exact value of the constant B. The reason is that these profiles are predominantly static in nature. In other words it means that the average Stark effect splitting, which is approximately equal to the half width of the higher series members, is significantly larger than the constants a_1 for

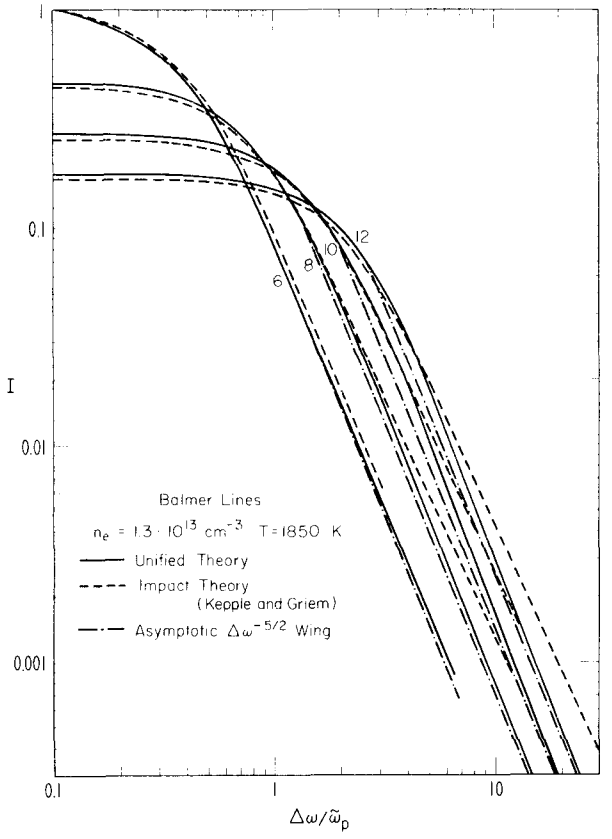

FIG. 8. Comparison between the unified theory and the modified impact theory of Kepple and Griem for the even Balmer lines H_6 to H_{12}.

the different Stark components (see equation (22)), which determine essentially the electron impact broadening. Since the line centers of the first series members are predominantly Doppler broadened, these low density experiments give no detailed information on the constant B. Hence, as one would expect, we also obtain a better agreement between theory and experiment than we did for the H_β- and H_γ-profiles discussed above, where the agreement could have been worse due to the uncertainty of the constant B. This fact is particularly important for astrophysical applications where one is mainly interested in low density profiles, because these profiles are insignificantly affected by the remaining uncertainty of the constant B. One may, therefore, calculate low density profiles with rather large confidence.

VI. DISCUSSION

Since the value of the constant B appears to be the most vague and restricting quantity in the current classical path theories, we will now summarize the effects which may influence the constant B and are not included in the present calculations. First of all, we can state

in general that the exact value of the constant B is least important if either the static broadening exceeds the electron impact broadening, as discussed above for the low density profiles, or if according to equation (22) the value of $\ln(4C^2)$ is much larger than the uncertainty of the constant B which means that

$$-\ln(4C^2) \gg 1. \tag{40}$$

According to equation (24) the latter situation is most likely to occur for the innermost Stark components of any hydrogen line.

The constant B is sometimes misleadingly referred to as the strong collision parameter. This is only partially correct, because its value depends not only on the lower cut off parameter $\rho_{\min}$ but also on the upper cut off parameter αD, where D is the Debye length and the constant α has been varied in the literature from 1.1[18] down to 0.6.[19] As discussed in the appendix of paper I, this parameter α will also influence the limits on the time integral $\int V(t')\,dt'$ in the time development operator $\mathcal{U}$ which for the S-matrix limit are extended from $-\infty$ to $+\infty$. In the unified theory calculations these limits have been extended from $-T$ to $+T$, where

$$T = \sqrt{(\alpha^2 D^2 - \rho^2)}/v, \tag{41}$$

in order to make the time limits consistent with the upper cut off parameter αD. We also saw from the appendix of paper I that, as a function of the parameter α, the constant B varies as

$$B = B(\alpha = 1) + 2\ln\alpha. \tag{42}$$

The correct value of the constant α has not yet been determined conclusively. Since for large impact parameters one is dealing only with weak collisions, it has to be possible to determine the parameter α from a second order classical path theory, which means essentially within the frame work of the ordinary impact theory.

The influence of small impact parameter collisions on the constant B is a much more involved problem. First of all, it is clear that one has to worry about collisions with impact parameters

$$\begin{aligned} \rho \gtrsim \rho_{\min} &= \lambda\!\!\!^{-} + \tfrac{3}{2}n^2 a_0 \\ &= \lambda\!\!\!^{-}(1 + 3.78 \cdot 10^{-3} n^2 \sqrt{T}) \end{aligned} \tag{43}$$

where classical path theories start to break down. As discussed for example, by SMITH[20] we have to distinguish in this range between "completed" strong collisions, which contribute primarily to the impact limit, and "incompleted" strong collisions, which mostly contribute to the static wings. While the latter collisions are properly treated in a classical path theory and have no influence on the value of the constant B, the "completed" strong collisions can only be treated correctly by a quantum mechanical calculation, which has not yet been done.

Besides the limitation imposed by a classical path approach, we also have to consider the influence of time ordering which has been neglected in our time development operator $\mathcal{U}$ of equation (5). We notice that time ordering will become important if $V\tau/\hbar \gtrsim 1$. With a typical collision time $\tau \simeq \rho/v$, this is the case for impact parameters

$$\rho \gtrsim \rho_{\text{ord}} = \tfrac{3}{2}(nq - n'q')\lambda\!\!\!^{-}. \tag{44}$$

For most practical cases, where the value of B becomes critical, ρ_{ord} is larger than ρ_{min}. Hence, there will be a domain, in which time ordering is important even within the region of validity of a classical path theory.

In the S-matrix limit the effect of time ordering has been investigated within the classical path theory for Ly_α[21] and for H_α[22] by solving the complete set of coupled differential equations, which define all the matrix elements of the time development operator. These calculations have demonstrated that the effect of time ordering may change the value of the constant B by as much as ± 1 and that the effect on the final line profile may amount to a few percent in intensity. These calculations have also included higher multipole terms. If one examines the effect of the higher multipole terms with respect to the case, where one considers only the dipole terms, one finds out that in case of Lyman $-\alpha$ as well as in case of H_α the higher multipole terms lower the value of all the different constants B. However, at the electron density and temperature of these experiments (which are essentially the same), the change in the constant B due to the higher order multipole terms affects the final line profile only very little.

For the more general case of the time development operator $\mathscr{U}$, required by the unified theory, the effect of time ordering has recently been examined for Lyman $-\alpha$[23]. These calculations show the results of the S-matrix limit in the line center and the decreasing influence of time ordering with increasing frequency perturbation $\Delta\omega$.

Due to the various outlined reasons which may affect the value of the constant B, it is rather difficult to make a quantitative statement of the possible error. If we assume that for impact parameters $\rho \gtrsim \rho_{ord}$ all the collisions which contribute to the value of B, have been treated correctly, one may give an upper bound on the possible error in B based on the unitarity condition of the time development operator. Since the time development operator may only oscillate within the limits of ± 1, the integral over impact parameters from 0 to ρ_{ord}, which is weighted by the impact parameter ρ, will change the constant B at the most by an amount of the order of unity. In addition to this the influence of the upper cut off parameter according to equation (42) has to be kept in mind. We also recall that in order to obtain the best agreement between theory and experiment we have to change the constant B for the Lyman α profile[14] by an amount which is slightly larger than 1, and for the H_β and H_γ profile by an amount, which is smaller than 1. It should also be noted that the ion field splitting is not fully taken into account in the time development operator as discussed in Section VI of paper I. It was shown that this may lead to slight modifications in the line center but not in the line wings. A full treatment would be rather difficult because the ion field exponentials in equation (VI.4) of paper I remove the spherical symmetry of the problem and a simple cut off procedure as suggested by KEPPLE and GRIEM[13] does not appear to be completely adequate since it affects the normalization of the line profile. In addition, near the line center we would expect the quasistatic description for the ions to be invalid. This, however, is practically unimportant because the Weisskopf frequency for the ions, which gives the range of validity for a quasistatic approach, is for low densities well inside the Doppler width and at high densities well inside the half width. Notice also that the breakdown of the no-quenching approximation may cause a small effect on the strong collision term (see Ref. 20, p. 315).

So far we have ignored profile asymmetries which have been observed, for example, in Ly-α, H_β and H_γ. In the following we give a brief discussion in which we do not consider the well known asymmetries due to the ω^4-factor in the expression for the power spectrum, the

frequency to wavelength conversion, and the Boltzmann factor,[24] which was neglected by assuming the elements of the atomic density matrix to be constant for all initial states. Asymmetries due to these effects will grow with increasing frequency perturbation $\Delta\omega$ and are always negligible in the line center. Hence, we are mainly concerned with the higher order multipole terms and the higher order Stark effect terms due to the electrons and ions.

In Section VII of paper I it was shown how the higher order multipole terms due to the electron perturbers can be included in the interaction potential of the time development operator and it was pointed out that within the no-quenching assumption only a finite number of multipole terms exist. The main aggravation is that the unitary transformation which diagonalizes the time development operator after the spherical average is no longer a simple rotation. In the impact limit this will affect primarily the constant B as noted above and cause only negligible asymmetries like in case of the time ordered solutions.[21,22]

The main reason for asymmetries especially in the line center has been shown to be due to the ions and we refer to a recent paper of SHOLIN[25] which supersedes the earlier papers by GRIEM[26] and NGUYEN-HOE *et al.*[27] In this paper, it has been successfully demonstrated that the observed asymmetries of the Ly-α, H_β and H_γ lines can all be explained within a static ion approach, where the main effect is caused by the quadrupole term of the ions and to a smaller extent by the quadratic Stark effect and the ion field dependent transition probability corrections of the individual Stark components. The electrons were assumed to cause only collision broadening and to introduce no further asymmetries.

It should be pointed out that the results presented by Sholin can easily be incorporated into the calculations presented here and work on this is in process. Like Sholin, we regard the radiator as being an atom in a static ion field ε_i and perturbed by the electrons. Hence, one only has to modify the matrix elements of $\Delta\omega_{\mathrm{op}}$ in equation (10) and of $\mathbf{d} \otimes \mathbf{d}$ in equation (25) according to the relations given by Sholin, in order to include the higher order multipole terms and the higher order Stark effect terms due to the static ions.

If we incorporate the higher multipole terms due to the electrons in the time development operator together with those due to the ions, another interesting feature of the unified theory is that a number of the higher order multipole terms due to the electrons and ions like, for example, the most important quadrupole terms, will cancel each other in the static limit of the electrons. This effect was already suspected by GRIEM[12] (p. 94). However, this sort of mutual compensation occurs only if electrons and ions are treated within the framework of the same approximations (for example, quasi-static or impact) as pointed out by SHOLIN.[25] For this reason the occurrence of asymmetries gives important information on the type of electron broadening. It is also clear why asymmetries have been observed in the high density profiles of Ly_α, H_β and H_γ, where the ions may be treated quasi-statically and the electrons are over most of the measured line profile in the domain of the impact theory, but not in the low density profiles of the higher Balmer and Paschen lines, where ions and electrons are both in the quasi-static domain over almost the entire line profile.

Finally, we may conclude that, at this stage, the accuracy of the unified theory calculations depends primarily on the extent to which the final line profile is affected by the constant B and to a lesser extent on the asymmetries not yet included. Both effects are in turn determined by the electron density and temperature. It is probably safe to say that in general the electron density obtained with the unified theory in its present form will differ at the most by 10 per cent from its true value. In the impact limit significantly better agreements between theory and experiment, which have been reported in the literature, have to

be regarded as fortuitous. However, better results are definitely obtained for the higher, still well isolated series members and/or at low electron densities ($n_e \lesssim 10^{13}$ cm^{-3}), which are of particular astrophysical interest.

REFERENCES

1. C. R. VIDAL, J. COOPER and E. W. SMITH, *JQSRT*, **10,** 1011 (1970).
2. E. W. SMITH, J. COOPER and C. R. VIDAL, *Phys. Rev.* **185,** 140 (1969).
3. J. W. B. HUGHES, *Proc. Phil. Soc.* **91,** 810 (1967).
4. H. A. BETHE and E. E. SALPETER, *Quantum Mechanics of One- and Two-Electron Atoms*. Springer-Verlag, Berlin (1957).
5. C. R. VIDAL, *Proc. of the 7th Intern. Conf. on Phenomena in Ionized Gases*, p. 168 (1966).
6. M. BARANGER and B. MOZER, *Phys. Rev.* **115,** 521 (1959); **118,** 626 (1960).
7. C. F. HOOPER, *Phys. Rev.* **165,** 215 (1968).
8. A. UNSÖLD, *Physik der Sternatmosphären*. Springer-Verlag, Berlin (1955).
9. F. N. EDMONDS, M. SCHLÜTER and D. C. WELLS, *Mem. R. Astr. Soc.* **71,** 271 (1967).
10. W. L. WIESE, D. E. KELLEHER and D. R. PAQUETTE, to be published. (The authors would like to thank Dr. Wiese for making his measurements accessible to us prior to publication).
11. W. L. WIESE, D. R. PAQUETTE and J. E. SOLARSKI, *Phys. Rev.* **129,** 1225 (1963).
12. H. R. GRIEM, *Plasma Spectroscopy*. McGraw-Hill, New York (1964).
13. P. KEPPLE and H. R. GRIEM, *Phys. Rev.* **173,** 317 (1968). See also Universty of Maryland, Report 831.
14. G. BOLDT and W. S. COOPER, *Z. Naturforsch.* **19a,** 968 (1964).
15. C. R. VIDAL, *Z. Naturforsch.* **19a,** 947 (1964).
16. H. SCHLÜTER, *Z. Naturforsch.* **15a,** 281 (1960).
17. R. D. BENGTSON, P. KEPPLE and J. D. TANNICH, *Phys. Rev.* **A1,** 532 (1970).
18. H. R. GRIEM, A. C. KOLB and K. Y. SHEN, *Astrophys. J.* **135,** 272 (1962).
19. W. R. CHAPPELL, J. COOPER and E. W. SMITH, *JQSRT*, **9,** 149 (1969).
20. E. W. SMITH, C. R. VIDAL and J. COOPER, *J. Res. Nat. Bur. Stand.* **73A,** 405 (1969).
21. M. BACON, K. Y. SHEN and J. COOPER, *Phys. Rev.* **188,** 50 (1969).
22. M. BACON, to be published.
23. T. GODFREY, C. R. VIDAL, J. COOPER and E. W. SMITH, *Phys. Rev.*, to be published.
24. D. L. HUBER and J. H. VAN VLECK, *Rev. Mod. Phys.*, **38,** 187 (1966).
25. G. V. SHOLIN, *Opt. Spectrosc.* **26,** 275 (1969).
26. H. R. GRIEM, *Phys. Rev.* **140,** A1140 (1965).
27. NGUYEN-HOE, H. W. DRAWIN and L. HERMAN, *JQSRT*, **4,** 847 (1964).
28. C. R. VIDAL, J. COOPER and E. W. SMITH, NBS Monograph 120 (1970).